Signatures of auroral potential structure extending through the near-equatorial inner magnetosphere

S. Imajo[1*], Y. Miyoshi[2], K. Asamura[3], I. Shinohara[3], M. Nosé[2], K. Shiokawa[2], Y. Kasahara[4], Y. Kasaba[5], A. Matsuoka[1], S. Kasahara[6], S. Yokota[7], K .Keika[6], T. Hori[2], M. Shoji[2], S. Nakamura[2], and M. Teramoto[8]

[1]Data Analysis Center for Geomagnetism and Space Magnetism, Graduate School of Science, Kyoto University, Kyoto, Japan

[2]Institute for Space-Earth Environmental Research, Nagoya University, Nagoya, Japan

[3]Institute of Space and Astronautical Science, Japan Aerospace Exploration Agency, Sagamihara, Japan

[4]Graduate School of Natural Science and Technology, Kanazawa University, Kakuma-machi, Kanazawa, Japan

[5]Graduate School of Science, Tohoku University, Sendai, Japan

[6]Graduate School of Science, University of Tokyo, Japan

[7]Graduate School of Science, Osaka University, Japan

[8]Kyushu Institute of Technology, Iizuka, Japan

Corresponding author: S. Imajo (imajo@kugi.kyoto-u.ac.jp)

†Additional author notes should be indicated with symbols (current addresses, for example).

Key Points: (max 140 char.)

- Signatures of an auroral U-shaped potential structure were found first in the near-equatorial inner magnetosphere by the Arase satellite.
- Upflowing ion beams, especially O^+ ion beams, were significantly deflected from field lines by a converging perpendicular electric field.
- The converging electric field and ion beam potentially affect the particle dynamics in the near-Earth plasma sheet.

Abstract

The auroral acceleration region plays an important role in the magnetosphere-ionosphere coupling system. In this study, signatures of an auroral U-shaped potential structure were found for the first time in the near-equatorial inner magnetosphere by the Arase satellite at ~6.0 R_E geocentric distance and 11˚ magnetic latitude. The observed magnetic and electric field variations corresponded to the equatorward motion of the upward field-aligned current and converging perpendicular electric field. Examining the three-dimensional velocity distribution function of H^+ and O^+ ions, we demonstrate that upflowing ion beams were significantly deflected in an east-west direction with a perpendicular velocity up to ~80 km/s, which is consistent with the ExB drift velocity. A simple particle drift model with the inferred auroral perpendicular potential presents a new kink-like drift path of ions from the magnetotail, implying that the auroral potential structure has a great impact on particle dynamics in the near-earth plasma sheet.

Plain Language Summary

The auroral arc involves multiple physical processes over a wide altitude range in the upper atmosphere. While the primary energy sources are at high altitudes, the accelerated electrons that are directly responsible for auroral emissions are mainly produced at lower altitudes. In the region where the electrons are accelerated downward, known as the auroral acceleration region, a peculiar electric field structure is formed. We clarified whether this electric field structure exists up to near the energy source region and how it affects the plasma dynamics by an in situ observation by the Arase satellite. We found for the first time that ions accelerated from below the satellite were supplied to the energy source region, and were deflected by the observed auroral electric field structure. Our model calculation shows that the electric field structure can significantly meander the motion of the entire near-Earth space plasma as it flows toward the Earth. Our result invites a new perspective that the structure of the electric field from low altitudes associated with the auroral arc has a significant impact on the dynamics of near-Earth space plasmas.

1 Introduction

The quasi-electrostatic electric field parallel to the magnetic field is a fundamental element of the auroral processes of discrete auroral arcs and the magnetosphere-ionosphere current systems. Typical phenomena observed on auroral arcs, such as a converging perpendicular electric field (Mozer et al., 1977), inverted-V shape energy spectra of downgoing electrons (Frank & Ackerson, 1971), and upflowing ion beams (Shelley et al., 1976), have supported the view of a U-shaped potential structure (e.g., Gurnett, 1972; Karlsson et al., 2020). Such a potential structure causes a decoupling of the plasma convection between above and below the region of the parallel electric field, known as the auroral acceleration region (e.g., Haerendel, 2007). Thus, the altitude at which the legs of the U-shaped potential surface extend is an important issue when considering the influence of the auroral potential structure

on the magnetospheric plasma dynamics. Janhunen et al. (1999) concluded that converging electric fields were rarely observed at geocentric distances above $4R_E$ using the POLAR satellite. They suggested that an O-shaped potential explains the low occurrence of high-altitude converging electric fields. In contrast, a more comprehensive study by Janhunen et al. (2004) found that the converging electric field could occur even at high altitudes when the geomagnetic activity is high. Recently, using the Arase satellite, Imajo et al. (2021) found a new acceleration region extending to very high altitudes; a converging electric field, ion beam, and satellite potential rise corresponding to an electron density decrease, as well as inverted-V like monoenergetic electrons and empty loss cones at a geocentric distance of 5.9 R_E around the plasma sheet boundary layer. These observations were made in the off-equatorial region; to date, it is not known whether the legs of the U-shaped potential structure extend throughout the entire field line to the equatorial magnetosphere.

There have been some studies of in-situ observations in the near-equatorial inner magnetosphere with conjugate discrete auroras; however, but there is a lack of the observational knowledge that related magnetospheric source processes to the aurora potential structure. Motoba, Ohtani, Anderson, et al. (2015) investigated the magnetospheric source region of growth phase/onset arcs using the Van Allen Probe B (RBSP-B) at a geocentric distance of ~5.0 R_E and magnetic latitude (MLAT) of ~10˚. With the RBSP-B, they observed an upward field-aligned current (FAC) located within the tailward part of a spatially localized plasma pressure peak, suggesting the role of local pressure gradients as a driver for the upward FAC in the arcs. Shiokawa et al. (2020) comprehensively analyzed the source region of auroral arcs during a substorm expansion phase using the Arase satellite at a geocentric distance of ~5.8 R_E and ~−17˚ MLAT. They found strong electric field fluctuations with large earthward/tailward Poynting fluxes and bidirectional electrons that can be considered as earthward plasma injections through the Fermi-type electron acceleration at energies above a few keV and upward field-aligned potential difference at energies below a few keV. However, evidence of a U-shaped potential structure extending to near the magnetic equator, such as a converging electric field accompanied by an inverted-V ion beam, has not been reported. If the auroral converging electric field can be mapped to the magnetic equator, substantial shear flows can exist and possibly play an important role in plasma transport processes. In addition, the fate of ion beams in the magnetosphere may be an important aspect of ion beams as seeds of background hot or energetic ions in the inner magnetosphere. Although statistical studies have shown that ion beams are common at high altitudes (> ~4 R_E geocentric distance) (Alm et al., 2015; Kondo et al., 1990), there has been no detailed analysis of the three-dimension velocity distributions of different ion species.

This paper aims to demonstrate how the structures and phenomena in the auroral flux tubes appear in the near-equatorial magnetosphere, based on comprehensive particle and field observations made by the Arase satellite. We use the observed electric field and ion beam energy, in addition to the model convection and corotation potential, to run a simple drift path model to evaluate the impact of the auroral potential structure on the plasma transport from the magnetotail into the inner magnetosphere during substorms.

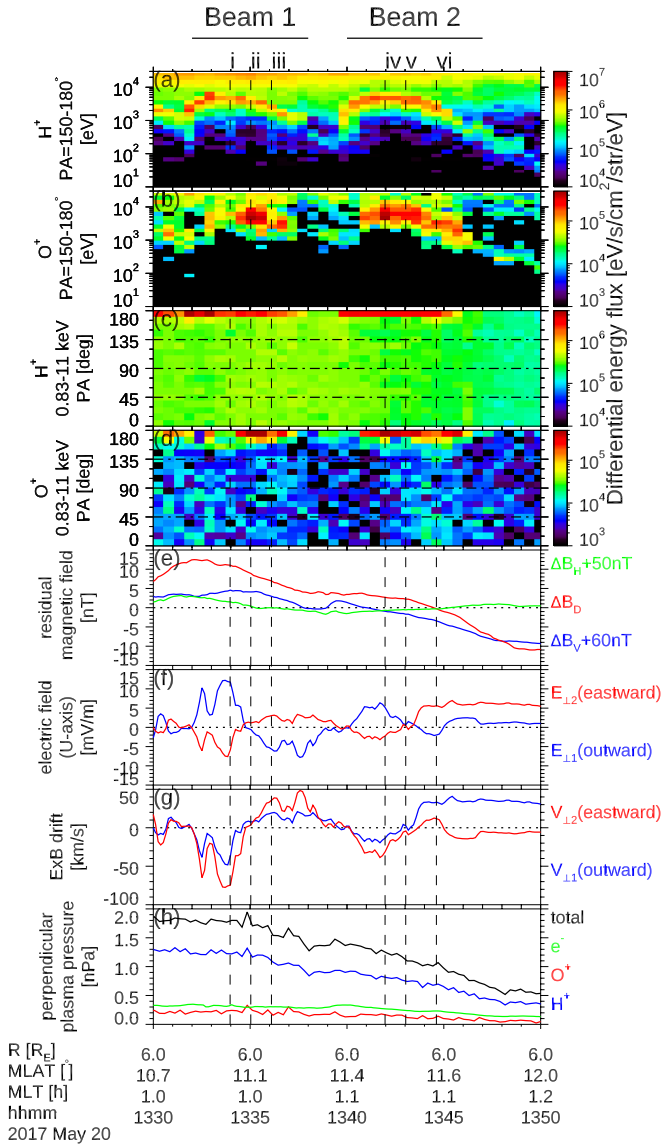

Figure 1. Overview of ion beam events on May 20, 2017, observed by the Arase satellite. Energy spectrum of (a) H^+ and (b) O^+ differential energy fluxes with a pitch angle range of 150˚–180˚. Pitch angle distribution of (c) H^+ and (d) O^+ differential energy fluxes with an energy range of 0.83–11 keV. (e) Residual magnetic fields subtracted by the IGRF model field and constant values in *VDH* coordinates. (f) Perpendicular electric fields and (g) ExB drift velocity calculated from the measured electric and magnetic fields. Blue and red lines indicate the eastward and outward components, respectively. (h) Perpendicular plasma pressure calculated from H^+ and O^+ ions with an energy range of 10–180 keV and electrons with an energy range of 7–88 keV. Blue, red, green, and black colors denote H^+ pressure, O^+ pressure, electron pressure, and their total, respectively. Vertical dashed lines are the time chosen for the snapshot of the velocity distribution in Figure 2.

2 Arase Observation of the near-equatorial inner magnetosphere

The Arase satellite has an elliptical orbit with a perigee of 400 km, an apogee of 32,000-km altitude, and an inclination of 31˚ (Miyoshi, Hori, et al., 2018; Miyoshi, Shinohara, et al., 2018). In this study, we analyzed the data from the instruments onboard Arase: the LEP-i for ions with an energy range of 0.6–25 keV (Asamura, Kazama, et al., 2018; Asamura, Miyoshi, et al., 2018), the MEP-i for ions with an energy range of 10–180 keV (Yokota et al., 2017, 2018), the MEP-e for electrons with an energy range of 7–88 keV (S. Kasahara, Yokota, Hori, et al., 2018; S. Kasahara, Yokota, Mitani, et al., 2018), the MGF for the magnetic field (Matsuoka et al., 2018a; 2018b), and the PWE/EFD for the electric field (Kasaba et al., 2017; Y. Kasahara et al., 2018).

On May 20, 2017, the Arase satellite at 6.0 R_E geocentric distance, 11˚ MLAT, and 1.1 h magnetic local time observed two consecutive ion beam events. Figure 1 shows an overview of these events. Inverted-V shape spectra are seen in the energy spectrum of upgoing H^+ and O^+ during 13:32–13:38 UT and 13:40–13:47 UT labeled by beams 1 and 2, respectively (Figures 1a and 1b). These inverted-V spectra indicate that the auroral acceleration region was located below the satellite altitude. Figures 1c and 1d show the pitch angle distributions of the H^+ and O^+ differential energy fluxes for each 10˚ bin. The H^+ beams were highly collimated along the field line within a 170˚–180˚ pitch angle, while the O^+ beams were spread over a wider pitch angle than H^+, consistent with early observations made at lower altitudes (Collin et al., 1981; Ghielmetti et al., 1986), which were interpreted in terms of species-dependent heating. Despite the relatively near-equatorial location, ion beams were unidirectional; that is, the satellite saw no ion beams coming from the southern hemisphere. To the best of our knowledge, no ion beam at very close to the magnetic equator (e.g., within ±5˚) has been reported. As discussed by Nosé et al. (2016) for energy-dispersed O^+ outflow in the inner magnetosphere, the unidirectional feature of the ion beams implies that some processes around the equatorial plane break the collimated beam distributions of ions and merge them into the background plasma.

Figure 1e shows the residual magnetic fields in *VDH* coordinates: *H* is antiparallel to the dipole axis, *V* is radially outward, and *D* is azimuthally eastward. The IGRF13 Earth's internal model field (Alken et al., 2021) and constant values for the baseline adjustment were subtracted from the measured field. The magnetic field showed a westward excursion in association with each ion-beam event. These magnetic variations corresponded to the satellite's outward (poleward) motion relative to the east-west-aligned upward current sheets typically accompanied by upflowing ion beams. Because the radial satellite motion in the rest frame was minimal (~0.4 km/s inward), the observed features were interpreted rather as the inward motion of two separated upward current sheets consecutively passing through the satellite.

The PWE/EFD instrument measures the electric field only in the satellite spin plane; thus here the electric field parallel to the spin axis is complemented by the assumption of relatively small electric fields parallel to $\boldsymbol{B}$, as $\boldsymbol{E} \cdot \boldsymbol{B} \approx 0$, where $\boldsymbol{E}$ and $\boldsymbol{B}$ are the electric and magnetic field vectors, respectively. The angle between $\boldsymbol{B}$ and the spin plane was ~75˚ during the event, which was sufficiently large to deduce the spin-axis component with this assumption. Then we

subtracted the $v \times B$ field due to the satellite orbital motion and the corotation electric field. We used the satellite-centered field-aligned coordinate system $(\mathbf{e}_{\perp 1}, \mathbf{e}_{\perp 2}, \mathbf{e}_{\parallel})$: the radially outward vector $\mathbf{e}_{\perp 1}$ is defined by $\mathbf{e}_{\phi_{SM}} \times \mathbf{e}_{\parallel}$, where $\mathbf{e}_{\parallel}$ is parallel to the magnetic field and $\mathbf{e}_{\phi_{SM}}$ is the azimuthally eastward direction in solar magnetic (SM) coordinates (equal to *D* in *VDH* coordinates), and the eastward vector $\mathbf{e}_{\perp 2}$ completes the orthogonal right-hand system. Figure 1f shows the electric field data. For beam 1, the outward electric field $(E_{\perp 1})$ variation from 12 to –8 mV/m was much stronger than the east-west variation ($E_{\perp 2}$) from -7 to 3 mV/m, indicating that the equipotential contours in the plane perpendicular to $\boldsymbol{B}$ were mostly east-west aligned. Beam 2 is also accompanied by at first a stronger outward electric field (6 mV/m) than the eastward electric field, but the eastward electric field became stronger than the former afterward. This change in the dominant field direction may be attributed to changes in the orientation of the auroral arc. The electric field was reversed from outward to inward near the center of the ion inverted-V structures (at times labeled by ii and v). This reversal is interpreted as a converging electric field that the satellite observed as it moved outward relative to the electric field structure. Figure 1g shows the flow velocity of the ExB drift derived from the observed magnetic and electric fields. Flow reversals occurred as expected from the electric field variation, and the eastward flow reached up to 80 km/s at the time labeled i and then reversed westward.

A possible magnetospheric closure of the FACs was the diamagnetic current driven by the pressure gradient. Figure 1h shows the perpendicular plasma pressure calculated from H^+ and O^+ ions at 10–180 keV and electrons at 7–88 keV. Note that these plasma pressures did not include those of the ion beam component below 10 keV. There was a decreasing trend during the plotted interval, but its slope slightly changed during both ion beams. The plasma pressure was relatively constant before and in the initial part of the ion beams, while its slope became larger after the initial part of the ion beams, implying that small pressure bumps are embedded in the equatorward side of the U-shaped potential structure. Although the pressure bump near the upward FAC region in the inner magnetosphere has been reported in the previous studies (Imajo et al., 2018; Motoba et al., 2015), the present study shows for the first time that pressure bumps are embedded near the U-shaped potential structure as well as the upward FAC.

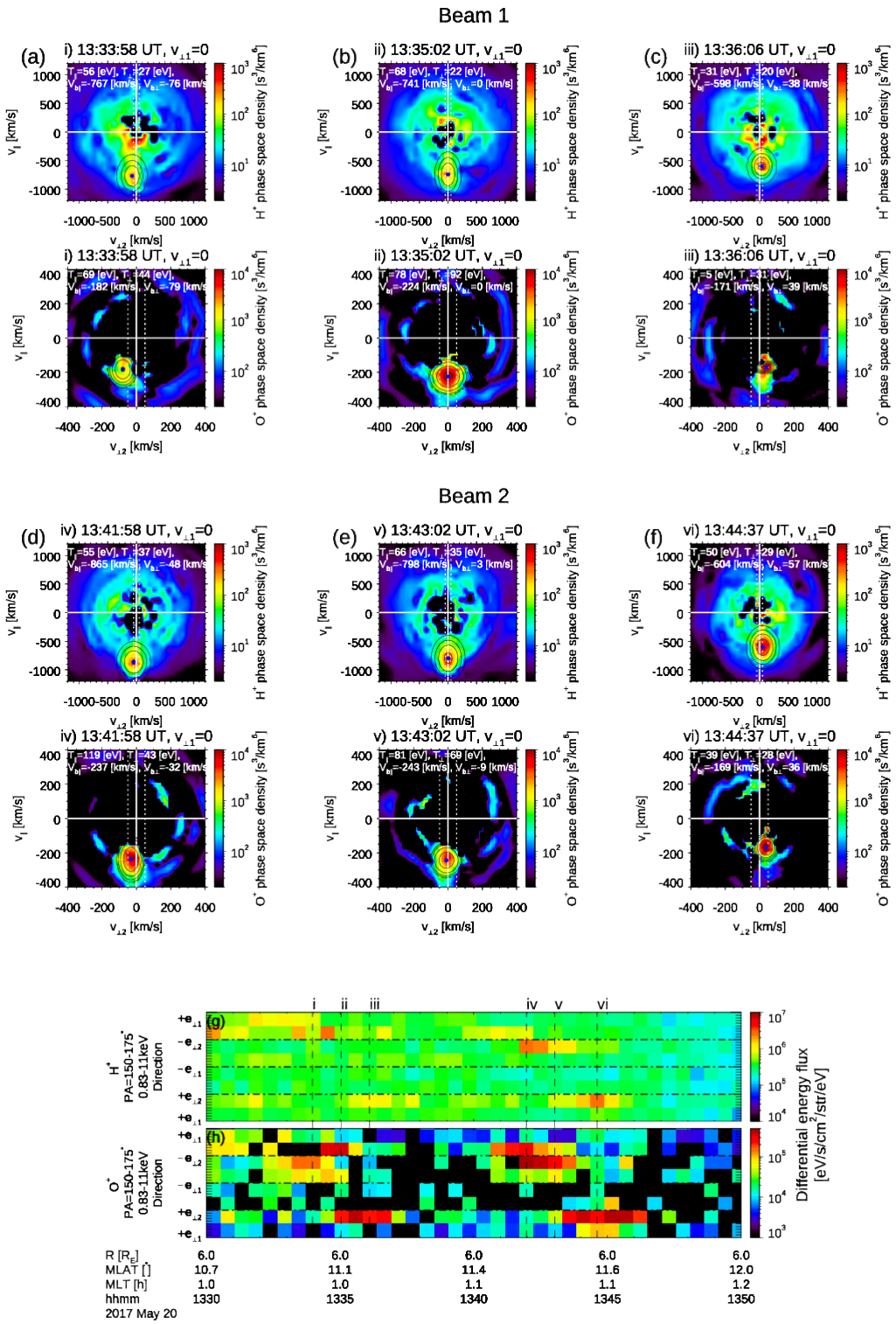

Figure 2. Three-dimensional distribution of ions in the satellite-centered field-aligned coordinate system. (a–f) Velocity distribution in the $\mathbf{e}_{\perp 2}$-$\mathbf{e}_{\parallel}$ plane of $V_{\perp 1} = 0$ (a, d) before, (b, e) near, and (c, f) after the electric field reversals at the center of converting electric fields during

the ion beam events. Top and bottom panels for each figure part indicate distributions of H^+ and O^+ ions, respectively. The time of each figure part corresponds to the vertical dashed lines labeled by i–vi in Figure 1. Vertical dashed lines show $\mathrm{V}_{\perp 2} = \pm 50\ \mathrm{km/s}$. The center and dispersion of the beam were estimated by fitting a shifted bi-Maxwellian function, and the fitted Maxwellian distribution and its peak location are drawn with black contour lines and blue dots, respectively. Values of center location (bulk velocity: V_b) and standard deviations (Temperature: T) of the fitted shifted bi-Maxwellian distribution are written by white texts in each plot box. Time series of the gyro phase distribution of (g) H^+ and (h) O^+ ions with a pitch angle of 150˚–175˚. Vertical dashed lines show the times for snapshots as a reference.

Here, we examine whether the electric field affects the motion of plasmas. The observed velocity distribution functions were interpolated over regular grids in the velocity space in the satellite-centered field-aligned coordinate system using ISEE3D (Keika et al., 2017) to visualize velocity distributions and estimate the beam center location. Figures 2a–2f show the velocity distributions of H^+ and O^+ ions in the $\mathbf{e}_{\perp 1}$-$\mathbf{e}_{\parallel}$ plane of $\mathrm{V}_{\perp 1} = 0$ before, near, and after the electric field reversals. The center of each beam was estimated by fitting a shifted bi-Maxwellian function to the interpolated velocity distribution. The perpendicular width of the beam was much smaller than that of the background ions, indicating that the beam is still colder (< 100 eV) than the background plasma sheet population. At the center of the U-shaped potential (Figures 2b and 2e), the ion beams were almost directed almost antiparallel to the magnetic field. For the first time, we find that the beam center is not always field-aligned; beams were deflected westward (Figures 2a and 2d) and eastward (Figures 2c and 2f), before and after the electric field reversals, respectively. The perpendicular velocity of the deflected beams was ~30–80 km/s, which is consistent with the estimated ExB drift velocity (Figure 1g). The deflection was more evident in the O^+ beams than the H^+ beams because the field-aligned velocity of the H^+ beams was 3–4 times larger than that of the O^+ beams while both species had a comparable perpendicular velocity. The difference in the parallel velocity was naturally expected from the field-aligned potential acceleration: it gives the same energy to ions with the same charge regardless of species, leading to slower parallel velocities for heavier ions, while the ExB drift gives the same perpendicular velocity. Figures 2g–2h show the time series of the gyrophase distribution of the ion beams. The westward ($-\mathbf{e}_{\perp 2}$) flux was dominant in the gyrophase before the electric field reversal, while the eastward ($+\mathbf{e}_{\perp 2}$) flux was dominant after the reversal. These features were somewhat more evident for O^+ beams owing to the larger deflection angle. Such a non-gyrotropic distribution can result in a significantly broadened pitch angle distribution if derived by simply averaging fluxes in each pitch angle bin in the rest frame, not in the ExB drifting frame, causing a wider pitch angle distribution of O^+ beams, as shown in Figure 1d. We simulated this effect using a simple model, as shown in Figure S1. The result indicates that the apparent broadening of the pitch angle distribution was not negligible if the ratio between perpendicular and parallel bulk velocities of a beam exceeded ~0.1.

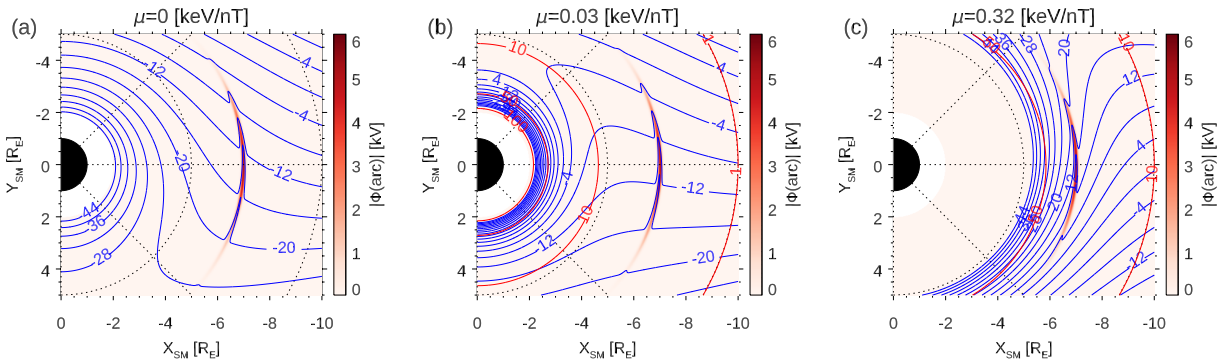

Figure 3. Guiding-center particle trajectory of single charged ions with 90˚ pitch angle in the localized auroral converging electric field, as well as the corotational electric field and Kp-dependent Volland-Stern convection electric field with Kp=4 at the event time. Magnetic moments were set to (a) 0, (b) 0.03, and (c) 0.32 keV/nT. Blue lines are drift paths, and red lines are the energy contour of particles in unit of keV. The background color shows the absolute value of modeled auroral potential drop given by a two-dimensional Gaussian function in the radial-azimuthal plane with the center at 7 Re midnight of –5 kV peak value and dispersions of 0.1 Re and 15˚.

3 Effects of the auroral converging electric field on particle trajectory

Using the Arase satellite observations, we demonstrated that the legs of U-shaped potential above the auroral acceleration region extended through the near-equatorial inner magnetosphere. Based on the proton beam energy, the potential difference between the edge and center of the auroral flux tube at the satellite altitude was estimated to be ~ –5 kV. Using a simple electric/magnetic field model, we examined the effect of this potential drop structure on the drift path of charged particles in the magnetic equatorial plane. Figure 3 shows the guiding-center trajectory of singly charged ions with different magnetic moments in the corotational electric field and Kp-dependent Volland-Stern convection electric field (Maynard & Chen, 1975; Stern, 1975; Volland, 1973) with a localized auroral converging electric field. The potential of the converging electric field was given by a two-dimensional Gaussian function of ρ (radial in X_{SM}-Y_{SM} plane) and ϕ (azimuthal), as $\Phi_{\mathrm{arc}}(\rho,\phi) = -5\exp\left(-\frac{(\rho-\rho_0)^2}{2\sigma_\rho^2} - \frac{(\phi-\phi_0)^2}{2\sigma_\phi^2}\right)$ [kV] with the center at 7 R_E around midnight (ρ_0 = 7 R_E and ϕ_0 =180˚) and standard deviations of σ_ρ =0.05 R_E and σ_ϕ =15˚. We used Kp =4, observed at the event time, for the Volland-Stern model. The magnetic moments were set to 0, 0.03, and 0.32 keV/nT, corresponding to energies of 0, 1, and 10 keV, respectively, and at a radial distance of 10 R_E in the Earth's dipole magnetic field. The maximum electric field for this potential drop was ~9.5 mV/m, which was similar to the observed value. The auroral converging electric field causes a kink-like drift path on the nightside in all cases; particles from the magnetotail drift eastward and then westward near the converging electric field region while convecting earthward. Energetic ions (10 keV, Figure 3c), they drift westward because of the magnetic gradient in the region beyond the U-shaped potential region and then eastward due to the inward electric field of the U-shaped potential region. Note that these kink-like drift paths may not be evident in the ionospheric plasma drift

due to the decoupling of the perpendicular electric field between above and below the acceleration region.

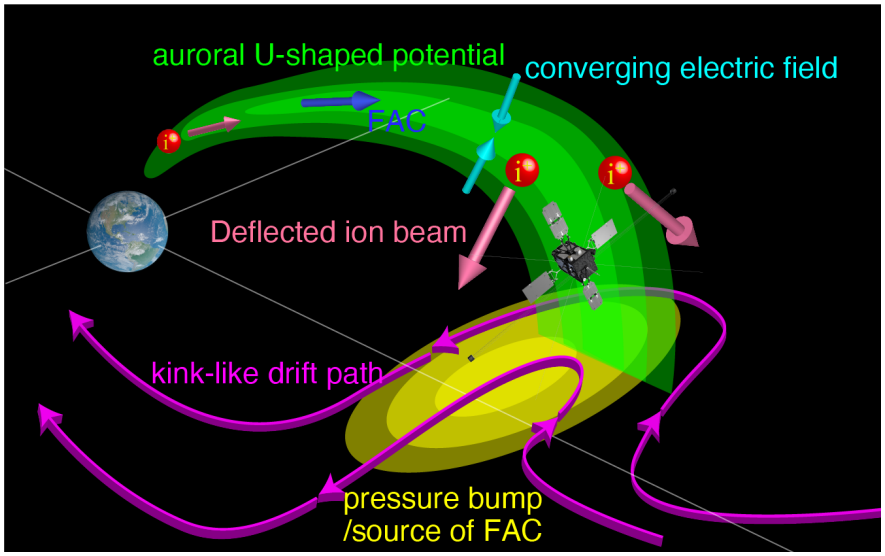

Figure 4. Schematic illustration of the auroral potential structure extending through the near-equatorial inner magnetosphere. The deflected ion beam corresponding to the converging electric field, the magnetic variations generated by the upward FAC, the plasma pressure bump considered as the source of the FAC were observed by the Arase satellite. The kink-like drift paths of the convecting plasma are indicated by purple streamlines.

4 Conclusions

Figure 4 is a schematic illustration of the auroral potential structure extending through the near-equatorial inner magnetosphere found by the Arase satellite observation. The Arase satellite at 6.0 R_E geocentric distance and 11˚ MLAT simultaneously observed upflowing H^+ and O^+ ion beams with converging electric fields, and upward FACs. The ion beams were deflected by the converging electric field and were thus not always exactly field-aligned. The O^+ ion beams have a larger deflection angles because their field-aligned velocity was slower than that of H^+ ions with a comparable perpendicular drift velocity. The perpendicular drift velocity of up to ~80 km/s in the magnetosphere is consistent with the ExB drift velocity estimated from the measured magnetic and electric fields. The azimuthal excursion of the magnetic field indicates that the FAC passed through the flux tube traversed by Arase. The perpendicular plasma pressure had a small bump during both ion beam events, and the resultant pressure-gradient perpendicular current partly contributed to the closure of the FAC. This result indicates that the legs of the U-shaped potential extended through the near-equatorial inner magnetosphere, that is, the auroral energy source in the magnetosphere, while the perpendicular electric field may not be fully mapped into the ionosphere owing to the non-equipotential field line associated with the auroral acceleration region. Such an electric potential can "kink" the drift path for charged particles from the magnetotail. Our results suggest that the auroral U-shaped potential structure has a signeficant impact on particle dynamics near-Earth plasma sheet via east-west flow shear corresponding to the converging electric field as well as the energetic ion

supply by field-aligned acceleration. Further quantitative studies are required to evaluate the impact of the potential structure and ion beam above auroral arcs on magnetospheric dynamics, such as plasma transport from the magnetotail into the inner magnetosphere during substorms.

Acknowledgments, Samples, and Data

The present study was supported by the Chubei Itoh Foundation, Grant-in-Aid for Young Scientists (21K13977), and JSPS, Grant-in-Aid for Scientific Research (20H01959, 15H05747, 16H06286, and 17H00728). M. Nosé is supported by JSPS, Grant-in-Aid for Scientific Research (B) (16H04057, 21H01147), and Specially Promoted Research (16H06286). Data from Arase used in this study are available from the ERG Science Center operated by ISAS/JAXA and ISEE/Nagoya University (https://ergsc.isee.nagoya-u.ac.jp/data_info/index.shtml.en). The present study analyzed L2 definitive orbit v03 data, LEP-i L2 v03.00 data and MEP-i L2 v01.01 data for protons and oxygen ions, MEP-e L2 v01.01 data for electrons, MGF L2 v03.04 spin-averaged data for the magnetic field data, and PWE/EFD L2 v05.01 data for the electric field data. The Kp index is available from the GFZ German Research Centre for Geosciences (Matzka et al., 2021). The software used to read and analyze the data, SPEDAS (Space Physics Environment Data Analysis Software) software package (Angelopoulos et al., 2019) including ERG plug-in tools (https://ergsc.isee.nagoya-u.ac.jp/erg_socware/erg_plugin/), is publicly available at http://themis.ssl.berkeley.edu/software.shtml and can be used without any restrictions.

References

Alken, P., Thébault, E., Beggan, C. D., Amit, H., Aubert, J., Baerenzung, J., et al. (2021). International Geomagnetic Reference Field: the thirteenth generation. *Earth, Planets and Space*, *73*(1). https://doi.org/10.1186/s40623-020-01288-x

Alm, L., Li, B., Marklund, G. T., & Karlsson, T. (2015). Statistical altitude distribution of the auroral density cavity. *Journal of Geophysical Research: Space Physics*, *120*(2), 996–1006. https://doi.org/10.1002/2014JA020691

Angelopoulos, V., Cruce, P., Drozdov, A., Grimes, E. W., Hatzigeorgiu, N., King, D. A., et al. (2019). *The Space Physics Environment Data Analysis System (SPEDAS)*. *Space Science Reviews* (Vol. 215). The Author(s). https://doi.org/10.1007/s11214-018-0576-4

Asamura, K., Kazama, Y., Yokota, S., Kasahara, S., & Miyoshi, Y. (2018). Low-energy particle experiments–ion mass analyzer (LEPi) onboard the ERG (Arase) satellite. *Earth, Planets and Space*, *70*(1), 70. https://doi.org/10.1186/s40623-018-0846-0

Asamura, K., Miyoshi, Y., & Shinohara, I. (2018). The LEPi instrument Level-2 3D flux data of Exploration of energization and Radiation in Geospace (ERG) Arase satellite.

Collin, H. L., Sharp, R. D., Shelley, E. G., & Johnson, R. G. (1981). Some general characteristics of upflowing ion beams over the auroral zone and their relationship to auroral electrons. *Journal of Geophysical Research*, *86*(A8), 6820. https://doi.org/10.1029/ja086ia08p06820

Frank, L. A., & Ackerson, K. L. (1971). Observations of charged particle precipitation into the auroral zone. *Journal of Geophysical Research*, *76*(16), 3612–3643. https://doi.org/10.1029/ja076i016p03612

Ghielmetti, A. G., Shelley, E. G., Collin, H. L., Sharp, R. D., Coilin, H. L., & Sharp, R. D. (1986). Ion specific differences in energetic field aligned upflowing ions at 1 R E (Vol. 38, pp. 77–82). https://doi.org/10.1029/GM038p0077

Gurnett, D. A. (1972). Electric field and plasma observations in the magnetosphere. In *Critical problems of magnetospheric physics* (p. 123).

Haerendel, G. (2007). Auroral arcs as sites of magnetic stress release. *Journal of Geophysical Research: Space Physics*, *112*(A9). https://doi.org/10.1029/2007JA012378

Imajo, S., Nosé, M., Matsuoka, A., Kasahara, S., Yokota, S., Teramoto, M., et al. (2018). Journal of Geophysical Research : Space Physics Magnetosphere-Ionosphere Connection of Storm-Time Region-2 Field-Aligned Current and Ring Current : Arase and AMPERE Observations. *Journal of Geophysical Research: Space Physics*, *123*(11), 9545–9559. https://doi.org/10.1029/2018JA025865

Imajo, S., Miyoshi, Y., Kazama, Y., Asamura, K., Shinohara, I., Shiokawa, K., et al. (2021). Active auroral arc powered by accelerated electrons from very high altitudes. *Scientific Reports*, *11*(1), 1–8. https://doi.org/10.1038/s41598-020-79665-5

Janhunen, P., Olsson, A., Mozer, F. S., & Laakso, H. (1999). How does the U-shaped potential close above the acceleration region? A study using Polar data. *Annales Geophysicae*, *17*(10), 1276–1283. https://doi.org/10.1007/s00585-999-1276-x

Janhunen, P., Olsson, A., & Laakso, H. (2004). The occurrence frequency of auroral potential structures and electric fields as a function of altitude using Polar/EFI data. *Annales Geophysicae*, *22*(4), 1233–1250. https://doi.org/10.5194/angeo-22-1233-2004

Karlsson, T., Andersson, L., Gillies, D. M., Lynch, K., Marghitu, O., Partamies, N., et al. (2020). Quiet, Discrete Auroral Arcs—Observations. *Space Science Reviews*, *216*(1), 1–50. https://doi.org/10.1007/s11214-020-0641-7

Kasaba, Y., Ishisaka, K., Kasahara, Y., Imachi, T., Yagitani, S., Kojima, H., et al. (2017). Wire Probe Antenna (WPT) and Electric Field Detector (EFD) of Plasma Wave Experiment (PWE) aboard the Arase satellite: specifications and initial evaluation results. *Earth, Planets and Space*, *69*(1), 174. https://doi.org/10.1186/s40623-017-0760-x

Kasahara, S., Yokota, S., Mitani, T., Asamura, K., & Hirahara, M. (2018). Medium - energy particle experiments — electron analyzer (MEP - e) for the exploration of energization and radiation in geospace (ERG) mission. *Earth, Planets and Space*, 1–16. https://doi.org/10.1186/s40623-018-0847-z

Kasahara, S., Yokota, S., Hori, T., Keika, K., Miyoshi, Y., & Shinohara, I. (2018). The MEP-e instrument Level-2 3-D flux data of Exploration of energization and Radiation in Geospace (ERG) Arase satellite. https://doi.org/10.34515/DATA.ERG-02000

Kasahara, Y., Kasaba, Y., Kojima, H., Yagitani, S., Ishisaka, K., Kumamoto, A., et al. (2018). The Plasma Wave Experiment (PWE) on board the Arase (ERG) satellite. *Earth, Planets and Space*, *70*(1), 86. https://doi.org/10.1186/s40623-018-0842-4

Keika, K., Miyoshi, Y., Machida, S., Ieda, A., Seki, K., Hori, T., et al. (2017). Visualization tool for three - dimensional plasma velocity distributions (ISEE _ 3D) as a plug - in for SPEDAS. *Earth, Planets and Space*. https://doi.org/10.1186/s40623-017-0761-9

Kondo, T., Whalen, B. A., Yau, A. W., & Peterson, W. K. (1990). Statistical analysis of upflowing ion beam and conic distributions at DE 1 altitudes. *Journal of Geophysical Research*, *95*(A8), 12091. https://doi.org/10.1029/ja095ia08p12091

Matsuoka, A., Teramoto, M., Imajo, S., Kurita, S., Miyoshi, Y., & Shinohara, I. (2018a). The MGF instrument Level-2 spin-fit magnetic field data of Exploration of energization and Radiation in Geospace (ERG) Arase satellite. https://doi.org/10.34515/DATA.ERG-06001

Matsuoka, A., Teramoto, M., Nomura, R., Nosé, M., Fujimoto, A., Tanaka, Y., et al. (2018b). The ARASE (ERG) magnetic field investigation. *Earth, Planets and Space*, *70*(1), 43. https://doi.org/10.1186/s40623-018-0800-1

Matzka, J., Bronkalla, O., Tornow, K., Elger, K., & Stolle, C. (2021). Geomagnetic Kp index. V. 1.0. GFZ Data Services. https://doi.org/10.5880/Kp.0001

Maynard, N. C., & Chen, A. J. (1975). Isolated cold plasma regions: Observations and their relation to possible production mechanisms. *Journal of Geophysical Research*, *80*(7), 1009–1013. https://doi.org/10.1029/JA080i007p01009

Miyoshi, Y., Shinohara, I., Takashima, T., Asamura, K., Higashio, N., Mitani, T., et al. (2018). Geospace exploration project ERG. *Earth, Planets and Space*, *70*(1), 101. https://doi.org/10.1186/s40623-018-0862-0

Miyoshi, Y., Hori, T., Shoji, M., Teramoto, M., Chang, T. F., Segawa, T., et al. (2018). The ERG Science Center. *Earth, Planets and Space*, *70*(1), 96. https://doi.org/10.1186/s40623-018-0867-8

Motoba, T., Ohtani, S., Anderson, B. J., Korth, H., Mitchell, D., Lanzerotti, L. J., et al. (2015). On the formation and origin of substorm growth phase/onset auroral arcs inferred from conjugate space-ground observations. *Journal of Geophysical Research: Space Physics*, *120*(10), 8707–8722. https://doi.org/10.1002/2015JA021676

Mozer, F. S., Carlson, C. W., Hudson, M. K., Torbert, R. B., Parady, B., Yatteau, J., & Kelley, M. C. (1977). Observations of paired electrostatic shocks in the polar magnetosphere. *Physical Review Letters*, *38*(6), 292–295. https://doi.org/10.1103/PhysRevLett.38.292

Nosé, M., Keika, K., Kletzing, C. A., Spence, H. E., Smith, C. W., MacDowall, R. J., et al. (2016). Van Allen Probes observations of magnetic field dipolarization and its associated O + flux variations in the inner magnetosphere at L < 6.6. *Journal of Geophysical Research: Space Physics*, *121*(8), 7572–7589. https://doi.org/10.1002/2016JA022549

Shelley, E. G., Sharp, R. D., & Johnson, R. G. (1976). Satellite observations of an ionospheric acceleration mechanism. *Geophysical Research Letters*, *3*(11), 654–656. https://doi.org/10.1029/GL003i011p00654

Shiokawa, K., Nosé, M., Imajo, S., Tanaka, Y. M., Miyoshi, Y., & Hosokawa, K. (2020). Arase Observation of the Source Region of Auroral Arcs and Diffuse Auroras in the Inner Magnetosphere Journal of Geophysical Research : Space Physics, 1–25. https://doi.org/10.1029/2019JA027310

Stern, D. P. (1975). The motion of a proton in the equatorial magnetosphere. *Journal of Geophysical Research*, *80*(4), 595–599. https://doi.org/10.1029/JA080i004p00595

Volland, H. (1973). A semiempirical model of large-scale magnetospheric electric fields. *Journal of Geophysical Research*, *78*(1), 171–180. https://doi.org/10.1029/JA078i001p00171

Yokota, S., Kasahara, S., Mitani, T., Asamura, K., & Hirahara, M. (2017). Medium-energy particle experiments – ion mass analyzer (MEP-i) onboard ERG (Arase). *Earth, Planets and Space*. https://doi.org/10.1186/s40623-017-0754-8

Yokota, S., Kasahara, S., Hori, T., Keika, K., Miyoshi, Y., & Shinohara, I. (2018). The MEP-i instrument Level-2 3-D flux data of Exploration of energization and Radiation in Geospace (ERG) Arase satellite. https://doi.org/10.34515/DATA.ERG-03000